ISBN: 978-3-95450-232-5 ISSN: 2673-7000 doi:10.18429/JACoW-NAPAC2022-WEPA43

SELF CONTAINED LINAC IRRADIATOR FOR THE STERILE INSECT TECHNIQUE (SIT)

A. Diego†*, R. Agustsson, R. Berry, S. Boucher, O. Chimalpopoca, S. Coleman[1], S. V. Kutsaev, A. Yu. Smirnov, V. Yu, RadiaBeam Technologies, Santa Monica, USA
[1]also at RadiaSoft, Boulder, USA

Abstract

A 3 MeV X-band linac has been developed employing a cost-effective split structure design in order to replace radioactive isotope irradiators currently used for the Sterile Insect Technique (SIT) and other applications. The penetration of a Co-60 irradiator can be matched with bremsstrahlung produced by a 3 MeV electron beam. The use of electron accelerators eliminates security risks and hazards inherent with radioactive sources. We present the current state of this X-band split structure linac and the rest of the irradiator system.

INTRODUCTION

Pest sterilization for insect population control has for decades used gamma irradiators with radioactive sources, however alternative sources have become available in part due to programs by the International Atomic Energy Agency. Sterile Insect Technique (SIT) is an important and environmentally conscious pest management technique developed and used for over 6 decades. SIT focuses on early incubation and sterilization of male insects at their pupa stage, thereby limiting a targeted insect's population when released into their natural habitat. To perform the sterilization, the pupae are placed in a canister in order to obtain a uniform dose ratio, with a target max/min dose ratio of approximately 1.3.

Currently, Co-60 isotope-based irradiators are commonly used for SIT. Although these Co-60 systems have been effective in pest control around the world, they are inherently costly to maintain and pose several safety concerns. In response to this problem, RadiaBeam is developing an inexpensive, compact 3 MeV split structure linac to act as the radiation source for a safe, self-contained irradiator for SIT and other applications. 3 MeV central energy was selected due to is similar output of the Bremsstrahlung spectrum produced by Co-60 isotope, 1.17 MeV and 1.33 MeV gamma particles [1]. Moreover, the X-band regime with a central frequency of 9300 MHz was chosen to reduce overall system dimensions, while exploiting the better RF consumption when compared to the more popular S-band systems [2].

Monte Carlo simulation show a dose uniformity ratio (DUR) less than 1.3 can be achieved for a 25 L water canister for a 3 MeV linac energy using an optimized tungsten and copper x-ray converter, and a 30-degree rms beam distribution. The overall system will take advantage of a beamline with a defocusing quadrupole magnet and a horn design to allow beam spread before the X-ray converter.

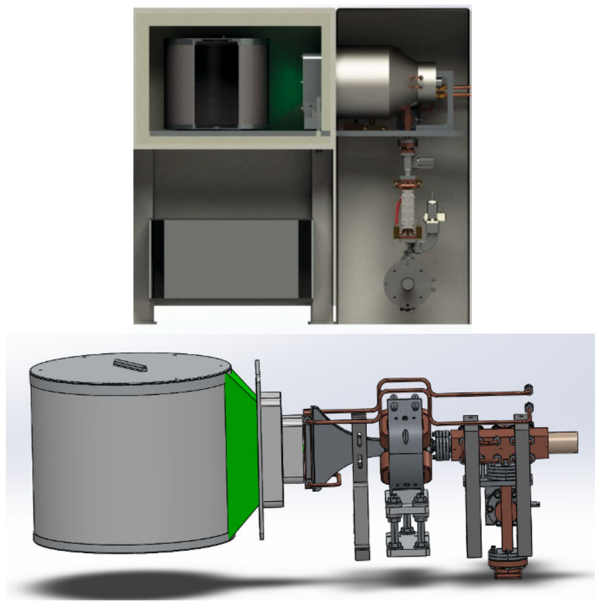

Figure 1: Conceptual design of SIT irradiation system (top), and designed accelerator section within SIT system (bottom).

Figure 1 illustrates the conceptual design layout for the SIT system (top), as well as a close up of the accelerating structure (bottom). We note the canister will be placed on a rotating plate (not shown) to allow unform dose distribution on the target pupa. The quadrupole, horn, converter, and collimation are shown in the bottom of Fig. 1 to illustrate the defocusing design and beam trajectory to achieve a DUR <1.3.

ACCELERATOR MANUFACTURING

To offset the cost of traditional high frequency accelerating structure manufacturing, RadiaBeam's SIT system design takes advantage of the split structure approach where two halves are brazed together rather than machining multiple single cells [3]. The full assembly consisted of three brazing steps, in which the planned brazing sequence ensures no piece of copper experiences more than three brazing cycles using a combination of gold (Au) and copper (Cu) alloys. This is to minimize the damage to the quality of the critical RF surfaces. In Fig. 2 we show the split structure halves post machining and fully assembled structure post final braze in Fig. 3.

* Work supported by US Department of Energy, SBIR grant no. DE-SC0020010.
† adiego@radiabeam.com

ISBN: 978-3-95450-232-5 ISSN: 2673-7000 doi:10.18429/JACoW-NAPAC2022-WEPA43

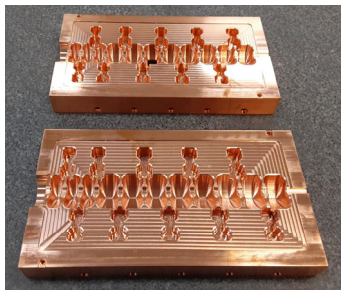

Figure 2: Post machined split structure halves.

After each braze cycle, Helium (He) leak tests were performed to ensure a hermitic structure, where no discernible leak above 1e-12 Torr/l*s was detected. Post braze RF cold measurements were successfully conducted and these tests are discussed in the subsequent section. We have also validated that the integrity of the split structure is not compromised when vacuum is pulled using a roughing pump.

In the current state, the structure has progressed to the electron gun installation. However due to supply shortages, we are currently waiting on an RF window, which in turn also places the gun installation on pause.

RF MEASUREMENTS

In addition to He leak checks after braze cycles, multiple RF cold tests were performed to ensure no gross deformities occurred due to high heat cycles. These cold tests included measurements of the operating frequency, Q-factor, coupling coefficient and on-axis field profile. The results were compared to CST simulations to demonstrate adequate agreement between simulations and measurements. Figure 3 shows the fabricated split structure post final braze during final RF cold tests.

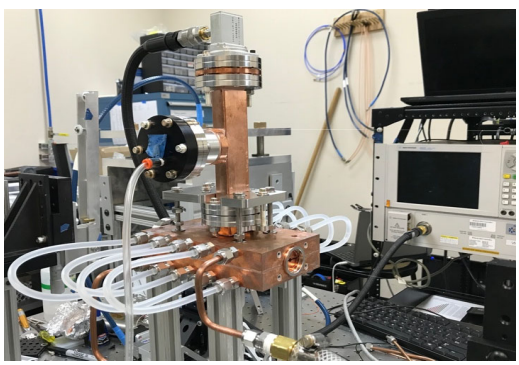

Figure 3: Fabricated split-structure undergoing RF measurements with water cooling and nitrogen gas flowing.

S11 was measured around 9300 MHz using with a vector network analyzer (VNA). To ensure thermal stability a chiller was used and set to 30 C during all RF cold tests, and additionally ultra-high purity Nitrogen gas (N2) was also used during testing. In addition to S11, on-axis field distribution at the operational π/2 mode with a standard bead pull procedure was also performed. The bead pull set up with the RF structure is shown in Fig. 3, and the measurement results are presented in Figs. 4 and 5.

An interesting effect was discovered after the second braze cycle. The center frequency was found at 9280.7 MHz, well below the target of 9300 MHz. Figure 4 shows the RF measurements at π/2-mode, with center frequency of 9280.7. During the analysis of these results, it was discovered that the frequency of the structure is sensitive to applied pressure on the two halves. Higher compression increased frequency, while decompression decreased frequency.

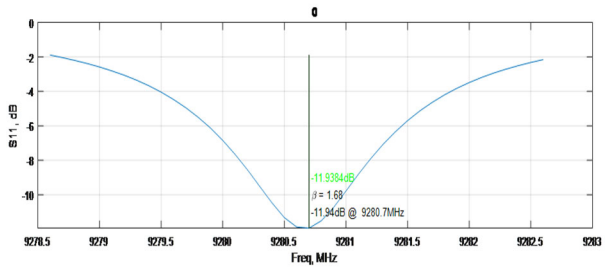

Figure 4: Measured S11 vs. frequency, π/2-mode centered at 9280.7 MHz.

To address the frequency shift due to compression, a bracket was designed to hold the coupling section in place and avoid detuning due to mechanical stress during installations. With the use of these brackets acting as strongbacks, we were able to tune the structure's frequency to 9289.2 MHz under dry N2, and expected 9291.8 MHz under vacuum. Figure 5 below show the resulting S11 and field profile with the mechanical brackets in place.

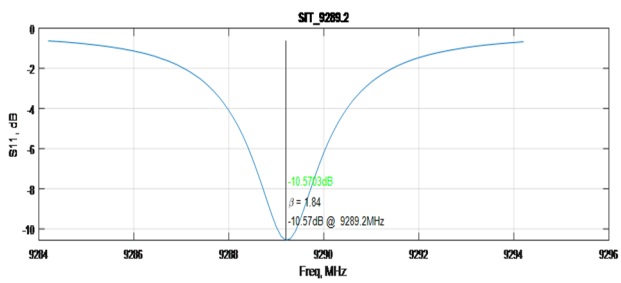

Figure 5: Measured S11 vs. frequency, π/2-mode centered at 9289.2 MHz.

Comparing the measured profiles from Figure with that in Figure there is a clear 9 MHz frequency increase that is closer to the target 9300 MHz. Additionally, the field in the bunching cells match the simulated profile better, and the field in the high energy cells of the structure (after cell #6) tend to decrease. The current RF measurement is acceptable for proper beam dynamics.

ISBN: 978-3-95450-232-5 ISSN: 2673-7000 doi:10.18429/JACoW-NAPAC2022-WEPA43

X-RAY CONVERTER

For the optimization of the X-ray target, we have chosen to use GEANT4-based Architecture for Medicine-Oriented Simulations (GAMOS) [4] and consequently have decided to use Tungsten (W) and Copper (Cu) layers for the 3 MeV linac target. As general practice for designing x-ray converters, a thin layer of high Z-material followed by a thick layer of lower Z-material is typically used [5,6]. The high Z-material thickness, in our case W, is first determined by finding the thickness that maximizes forward x-ray production. The thickness of the second lower Z material of Cu, is found by ensuring that primary electrons from the incident electron beam are stopped from reaching the irradiating canister [7].

Optimization of the target took place in two steps, first the W-thickness was optimized by finding the maximum X-Ray dose produced as function of W-thickness with the 3 MeV incident electron beam. Secondly, the Cu-thickness as a function of measured electron dose was examined while maintaining a constant W-thickness.

Results for optimal W target thicknesses are illustrated in the graph from Fig. 6. The graph demonstrates the X-ray dose measured by the water phantom as function of increasing W thickness. Results indicate a maximum X-ray dose was produced with a W thickness of .4 mm; the peak points are highlighted with the grey box for visibility. We can see that at these points, X-ray dose plateaus and begins to decrease after .42 mm.

Obtaining a W thickness of .4 mm can be readily done, as we have located W foil with thicknesses of .015" (.381 mm), and .0008" (.0203 mm) that allows us to create the W thickness needed. Moreover, there is little difference in the dose produced from .40 mm and .42 mm of W, which allows us to use two standard W foil sizes. With the W thickness found, the absorber layer of Cu was investigated.

To do this, a constant .4 mm W thickness was kept in place, and backed by an increasing Cu absorber layer. The Cu thickness was increased from .1 mm to 1.4 mm in steps of .02 mm. Simulation results indicate that a minimum Cu thickness of 1.1 mm is needed to minimize primary electrons from reaching the irradiated material.

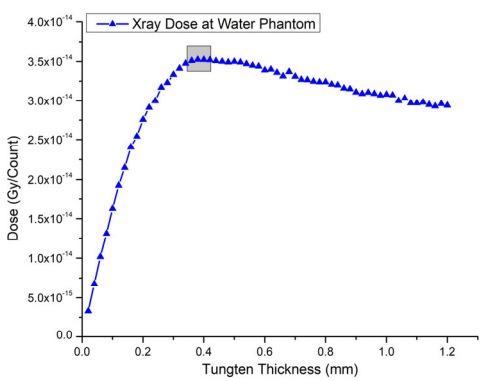

Figure 6: Plotted dose data used to determine optimal thickness needed for Tungsten layer.

In its current design, the converter will come together through a series of brazing and welding operations. First, the converter target is brazed using Au-Cu braze alloy. The brazing operations sets the tungsten target in the copper backplate and integrates the direct cooling channels to the sub-assembly. The design will implement a horn aperture to allow maximum defocusing from a quadrupole. The conceptual design is shown in Fig. 7, we note a ceramic break is used to isolate the converter from the linac, which will allow us to measure the relative beam current once testing begins.

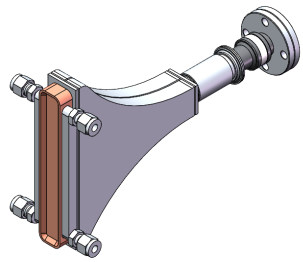

Figure 7: SIT system full converter design.

Thermal simulations have also been performed using COMSOL Multiphysics. The volumetric heating power is derived using the incident electron beam and the stopping power of the material. We define the convertor structure with its constituent materials and their thermal properties. The above derived heat source is imposed on the structure. Film coefficients are applied along the cooling channel surfaces with values matching realistic scenarios.

The simulation is conducted with two approaches: one-shot extrapolation and steady state approximation. In the one-shot case, one pulse of the beam is incident on the structure and the thermal response is simulated over a long period of time. In the steady state approximation approach, the heat is continuously imposed at a fraction of the intensity of a pulse matching its duty cycle.

The two approaches give very similar results. In both cases, no point in the converter has an end temperature that exceeds 100 Celsius. The structural integrity of the convertor is not threatened, and there will be no boiling issues with water cooling.

CONCLUSION

We have manufactured and cold tested a 3 MeV split structure linac to replace the use of Co-60 gamma ray irradiators used for the sterile insect technique. Post final braze RF cold tests show the accelerator has a center frequency of 9289.2 MHz under dry N2, and beam dynamics show this frequency and the measured field profile will yield the required beam energy and current. The next steps, planned later this year, are to weld on the electron gun, carry out RF conditioning, and measure the electron beam parameters.

ACKNOWLEDGEMENTS

This work was financed by the US Department of Energy, SBIR grant no. DE- SC0020010.

ISBN: 978-3-95450-232-5 ISSN: 2673-7000 doi:10.18429/JACoW-NAPAC2022-WEPA43

REFERENCES

[1] K. D. Steidley and C. W. Rosen, "Dosimetric aspects of a 3.3-MV linear accelerator," in *Medical Physics*, vol. 17, no. 3, pp. 474-480, 1990. doi:10.1118/1.596487

[2] S. Kutsaev, R. Agustsson, R. Berry, S. Boucher, and A. Smirnov, "Electron Accelerator for Replacement of Radioactive Sources in Insect Sterilization Facilities," *Physics of Atomic Nuclei*, vol. 84, no. 10, pp. 1743-1747, 2021. doi:10.1134/S1063778821100215

[3] R. Agustsson, S. Boucher, and S. Kutsaev, US Patent No. WO2020061204A1, 2019.

[4] GAMOS, *Fismed. Ciemat. Es*, 2022, http://fismed.ciemat.es/GAMOS/gamos.php

[5] Q. Gao, H. Zha, H. B. Chen, and J. Shi "Design and Optimization of the Target in Electron Linear Accelerator", in *Proc. IPAC'13*, Shanghai, China, May 2013, pp. 3663-3665.

[6] P. Buaphad *et al.*, "X-ray Dose Rate of 6/4 MeV European S-band Linac Structure for Industrial Application at RTX", in *Proc. IPAC'19*, Melbourne, Australia, May 2019, pp. 3494–3496. doi:10.18429/JACoW-IPAC2019-THPMP021

[7] R. B. Miller, *Electronic Irradiation of Foods*. New York, NY: Springer, 2010.